BIOORGANIC CHEMISTRY 20, 8–29 (1992)

Potential ATPase Mimics by Polyammonium Macrocycles: Criteria for Catalytic Activity[1,2]

ANDREA BENCINI,* ANTONIO BIANCHI,* ENRIQUE GARCIA-ESPANA,† EDMUND C. SCOTT,‡ LUIS MORALES,‡ BINGHE WANG,‡ TAMBOUE DEFFO,‡ FUSAO TAKUSAGAWA,‡ MATHIAS P. MERTES, KRISTIN BOWMAN MERTES,‡ AND PIERO PAOLETTI*

*Chemistry Department, University of Florence, via Maragliano 75/77, 50144 Florence, Italy;† Inorganic Chemistry Department, University of Valencia, c/Dr. Moliner 50, 46100 Burjasot, Valencia, Spain and ‡Departments of Chemistry and Medicinal Chemistry, University of Kansas, Lawrence, Kansas 66045.

Received March 18, 1991

A series of polyammonium macrocycles, ranging in size from the 18-membered ring [18]aneN$_6$ to the 36-membered [36]aneN$_{12}$ were examined as potential ATPase mimics. The rates of hydrolysis of ATP were followed at pH 3.0 and 7.0 using ^{31}P NMR and HPLC techniques. Stability constants as a function of degree of protonation, distribution curves for the ligands as a function of pH, and distribution curves for the mixed species of nucleotides, inorganic phosphate, and macrocycle were also determined. All of the macrocycles catalyzed the hydrolysis of ATP to some extent compared to noncatalyzed hydrolysis. A critical dependence on macrocyclic ring size was observed, with [21]aneN$_7$ being the best catalyst at both pHs. Stability constants of the complexes formed between the phosphate species and macrocycle increase with increasing degree of protonation and decreasing ring size. The trend in stability constants for phosphate species was found to be $PO_4^{3-} > P_2O_7^{4-} > ATP^{4-} > ADP^{3-} > AMP^{2-}$ for a given degree of protonation. The crystal structure of tetraprotonated [21]aneN$_7$ was determined. The compound $N_7C_{14}Cl_4H_{41}O$ crystallizes in the monoclinic space group $P2_1$ (#4) with unit cell dimensions a = 7.472(1), b = 19.480(2), c = 8.3638(9) Å, β = 100.38(1)°, and V = 1197.4(3)Å^3. The structure was solved by direct methods and refined using full-matrix least-squares techniques to give a final R = 0.041 and R_w = 0.055.

INTRODUCTION

Polyammonium macrocycles are astoundingly successful mimics of a variety of phosphoryl transfer enzymes (1–3). These simple cyclic compounds are noted for the capability to bind to a number of anions, including the simple phosphates and polyphosphates as well as more complex nucleotides. One of the most widely studied macrocycles in this area is the 24-membered 1,13-dioxa-4,7,10,16,19,23-hexaazacyclotetracosane, [24]aneN$_6$O$_2$, which has been found to exhibit both ATPase (*1*) and kinase activity (*2, 3*). Mechanistically, covalent catalysis plays an

[1] Dedicated to the memory of Mathias P. Mertes.

[2] Supplementary material, including tables of structure factors, anisotropic thermal parameters, and hydrogen atom parameters, is available from Kristin Bowman Mertes.

0045-2068/92 $3.00

important role, via the formation of an intermediate macrocyclic-phosphoramidate species in aqueous solution, which is subsequently hydrolyzed (*1*), or can be transferred to another anion such as phosphate (*2*) or formate (*3*). In order to explore the influence of ring size on this reaction, a variety of polyamine macrocycles ranging in size from the 21-membered [18]aneN$_6$ to the 36-membered [36]aneN$_{12}$ **(1)** were examined for their catalytic aptitude. The results were then compared to the degree of complex formation as obtained from the stability constants at a variety of pHs, as well as to structural considerations from the crystal structure of [21]aneN$_7$. The main aim of this work is to study the relationship between the species present in solution (i.e., the composition of the solutions) and the kinetics of ATP hydrolysis using a series of polyazacycloalkanes of the type [3*k*]aneN$_k$ (k = 6–12):

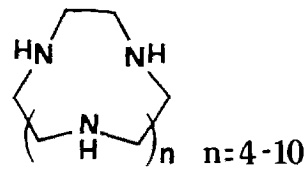

1

EXPERIMENTAL

Materials. The sodium salts of ATP, ADP, and AMP were obtained from Boehringer-Mannheim. The large polyazacycloalkanes and their hydrochloride salts were obtained as previously reported (*4–8*). The macrocycle [18]aneN$_6$ was purchased from Aldrich or Fluka and used as its hexahydrochloride salt. Satisfactory elemental analyses were obtained for all the compounds. All the potentiometric measurements were carried out in 0.15 mol dm^{-3} $NaClO_4$, which was used as a supporting electrolyte and was purified according to a published procedure (*9*). CO_2-free NaOH and HCl solutions were also prepared according to established procedures (*10*). All other chemicals used were high purity commercial products.

Synthesis of N-phosphoryl [21]aneN$_7$. A modified procedure of Benkovic and Sampson was used (*11*). Diphenyl chlorophosphate (360 μl, 0.017 mmol) was added slowly with stirring to the free amine [21]aneN$_7$ (105 mg, 0.348 mmol) in 3 cm^3 $CHCl_3$ cooled in an ice bath. After addition was complete, the reaction mixture was stirred at room temperature for 4 h, followed by addition of 10 cm^3 of 1 mol dm^{-1} HCl. The $CHCl_3$ layer was separated, and the aqueous layer was washed with $CHCl_3$ (3 × 10 cm^3) and evaporated to dryness, yielding the *O,O*-diphenylphosphoramidate of [21]aneN$_7$ as a foam in 47% yield. ^{1}H NMR (D_2O)δ 8.05–7.26 (10H, m, aromatic), 3.46–2.76 (28H, m, NCH_2) ppm; ^{13}C NMR (D_2O)δ 133.10, 129.14, 123.07, 47.25, 46.88, 46.78, 46.71, 46.47, 46.28 ppm; HRMS (FAB from thioglycerol/glycerol matrix) *m/e* for $C_{26}H_{44}N_7O_5P$ (*M* + 1) requires 534.3321. Found 534.3339.

The diphenylphosphoramidate (162 mg, 0.30 mmol) was dissolved in 2 cm^3 of 10 mol dm^{-3} KOH and refluxed for 10 min in a preheated oil bath at 130°C. After

refluxing the reaction was quickly cooled in ice and the pH adjusted to 7 using either 17.4 mol dm^{-3} CH_3COOH or 12 mol dm^{-3} HCl to give the phosphoramidate of [21]aneN_7. This compound was too unstable to obtain a complete analysis: ^{31}P NMRδ 9.837 ppm.

METHODS

Emf measurements. The potentiometric measurements were carried out using equipment (potentiometer, cell, buret, stirrer, microcomputer, etc.) that has been fully described (*12*). The reference electrode was Ag/AgCl in saturated KCl solution. The glass electrode (Orion Model 91-01) was calibrated as a hydrogen concentration probe, by titration of well-known amounts of HCl with NaOH solution, determining the equivalent point by the Gran method (*13*), which provides the standard potential of the cell ($E°$) as well as the ionic product of water (pK_w = 13.73(1) in 0.15 mol dm^{-3} $NaClO_4$ at 298.15 K). The protonation constants of the ligands in this study have been previously reported (*6–8, 14*), as well as those of ATP^{4-} (*15, 16*). The protonation constants of AMP^{3-}, ADP^{2-}, PO_4^{3-}, and $P_2O_7^{4-}$ have been redetermined for our experimental conditions. In the system [21]aneN_7-ATP the pH-range studied was 4.5–9.5 because of the high hydrolytic rate of ATP at lower pH values. For the system [18]aneN_6-ATP the pH-range studied was 4.7–9.3 due to precipitation at lower pH values. The program SUPERQUAD (*17*) was used to calculate the stability constants. The titration curves for each system were treated either as a single set or separately without significant variations in the values of the stability constants. Furthermore, the sets of data were merged together and treated simultaneously to give the final stability constants. Owing to the large number of species formed in these systems, great care has to be taken in the selection process for the equilibrium model [see Ref. (*8*), note 18].

NMR kinetic analysis. ^{31}P NMR spectra were recorded at 121.42 MHz on a Varian XL300. Chemical shifts in ppm are relative (+, downfield) to an external reference of 85% H_3PO_4. Probe temperature was regulated by a variable temperature accessory. The use of low decoupler power for heteronuclear decoupling at the reported concentrations of reagents and salts in 5 mm NMR tubes did not result in apparent temperature variations.

The solution pH was recorded at 22°C using a Radiometer pH meter. Adjustments to the desired pH of 0.5-cm^3 samples containing the ligand and substrate were made using ~5 mol dm^{-3} NaOH or HCl. Kinetic studies were performed by following the time-dependent change in the integrals from the resolved ^{31}P NMR signals of P_α, P_β, and P_γ of ATP and peaks for inorganic phosphate and the phosphoryl derivatives of the macrocycles, when phosphoramidates were formed. Calibration curves were employed when the integral ratios were not equal because of variations in the ^{31}P relaxations times. By this method of analysis the calculated standard deviation for the observed rates was 6%.

In a typical experiment, a 0.5-cm^3 solution containing ATP, the polyamine as its hexahydrochloride salt in 10% D_20/H_2O (0.02 mol dm^{-3}) in each, was placed in the NMR probe in a 5-mm tube. The temperature was then brought to the

TABLE 1

Crystallographic Data for [21]aneN$_7$

Compound	$N_7C_{14}Cl_4H_{41}O$
fw	465.34
a(Å)	7.472(1)
b(Å)	19.480(2)
c(Å)	8.3638(9)
β(deg)	100.38(1)
V(Å^3)	1197.4(3)
ρ calcd. (g cm^{-3})	1.291
Z	2
Space group	$P2_1$ (#4)
Crystal dimensions (mm)	0.500 × 0.200 × 0.010
Temp. (°C)	20
Radiation	CuK_α
Diffractometer	Rigaku AFC5R
μ (cm^{-1})	47.39
2θ range (deg)	0.43
No. independent reflections	1627
No. with $I > 3\sigma(I)$	1597
Final R	0.041
Final R_w	0.055

desired value. By the use of an automated program, an adequate number of acquisitions were accumulated for each sequential spectrum over a period of several half-lives.

HPLC kinetic analysis. A Waters Model 501 high performance liquid chromatograph together with Waters Model 481 (absorbance detector) and 740 data analyzer was used in these studies. Samples were injected on a silica column containing amine groups (Waters Bondpak-NH_2) which, in the reverse phase of operation, gives an ion-exchange-based separation. The mobile phase was a mixture of 15% acetonitrile and 85% 0.05 mol dm^{-3} ammonium phosphate at pH 4.5.

Aqueous solutions of the substrates and macrocycles in concentrations of 1 μM were examined at 70°C with the pH adjusted as described in the NMR studies. Samples were analyzed by first quenching 20-μl aliquots of the reaction mixture by addition to 40 μl of the mobile phase adjusted to pH 10.5 prior to injection. Resolution of AMP, ADP, and ATP afforded integrals used in the determination of the concentrations of the individual adenine containing species at each time point. Analysis was based on multiple samples accumulated over several half-lives.

X-ray data. Crystal structure information is given in Table 1. Crystals suitable for X-ray analysis were obtained by recrystallization of the hydrochloride salt from a water–methanol mixture. A transparent plate of [21]aneN$_7$ was mounted on a glass fiber. A Rigaku AFC5R diffractometer with graphite monochromated CuK_α radiation (λ = 1.5405 Å) and a 12-kW rotating anode generator were used to collect the data. Cell constants and an orientation matrix for data collection were obtained

from a least-squares refinement of 20 carefully centered reflections in the range $69.30° < 2\theta < 69.90°$. The compound crystallizes in the monoclinic system $P2_1$ with the systematic absence $0k0\ k \neq 2n$. The data were collected at a temperature of 20 ± 1°C using the ω-2θ scan technique to a maximum 2θ value of 112.6°. Omega scans of several intense reflections, made prior to data collection, had an average width at half-height of 0.43° with a take-off angle of 6.0°. Scans of (1.52 + 0.30 tan θ)° were made at a speed of 32.0°/min (in ω). The weak reflections ($I < 10.0\sigma(I)$) were rescanned (maximum of two rescans) and the counts were accumulated to assure good counting statistics. Stationary background counts were recorded on each side of the reflection. The ratio of peak counting time to background counting time was 2 : 1. The diameter of the incident beam collimator was 0.5 mm and the crystal to detector distance was 285.0 mm.

Of the 1765 reflections which were collected, 1627 were unique ($R_{int} = 0.074$). Equivalent reflections were merged. The intensities of three representative reflections, which were measured after every 99 reflections, remained constant throughout data collection. No decay correction was applied. An empirical absorption coefficient, based on azimuthal scans of several reflections, was applied ($\mu = 47.4$ cm^{-1}). Transmission factors ranged from 0.52 to 1.00. The data were corrected for Lorentz and polarization effects.

Solution and refinement. The structure was solved by direct methods (*18*). The nonhydrogen atoms were refined anisotropically. The final cycle of full-matrix least-squares refinement was based on 1597 observed reflections ($I > 3.00\sigma(I)$) and 398 variable parameters and converged (largest parameter shift was 0.72 times its e.s.d.) with $R = \Sigma||F_o| - |F_c||/\Sigma|F_o| = 0.042$ and $R_w = [(\Sigma w(|F_o| - |F_c|)^2/\Sigma wF_o^2)]^{1/2} = 0.055$. The goodness of fit was 1.19. The weighting scheme was based on counting statistics and included a factor ($p = 0.10$) to downweight the intense reflections. The maximum and minimum peaks on the final difference Fourier map corresponded to 0.29 and -0.39 $e^-/Å^3$, respectively. Neutral atom scattering factors were taken from Cromer and Waber (*19*). Anomalous dispersion effects were included in F_{calc} (*20*). The values for $\Delta f'$ and $\Delta f''$ were those of Cromer (*19*). All calculations were performed using the TEXSAN crystallographic software package (*21*).

RESULTS AND DISCUSSION

Stability Constants

In Tables 2, 3, and 4 are presented the stability constants, experimentally determined in this work, relative to the interaction of the so-named "large" polyazacycloalkanes (*4*) of the variously protonated series $[3k]aneN_k$ ($k = 7$–11) with the anions ATP^{4-}, PO_4^{3-}, and $P_2O_7^{4-}$. These are all constants reported for the first time. The constants associated with the interaction of $H_n[21]aneN_7^{n+}$ with ADP and AMP as well as those of $H_n[18]aneN_6^{n+}$ with ATP have also been included in Table 2. Although the formation in some cases of both 1 : 1 and 2 : 1 anion–macrocycle complexes has been observed (*22*), the data analysis with the program

TABLE 2

Logarithms of the Stability Constants for the Interaction ATP-[3*k*]aneN$_k$ (k = 6–12) in 0.15 mol dm^{-3} $NaClO_4$ at 298.15 K

Reaction	[18]aneN$_6$ ATP^{4-}	[21]aneN$_7$ AMP^{2-}	[21]aneN$_7$ ADP^{3-}	[21]aneN$_7$ ATP^{4-}	[24]aneN$_8$ ATP^{4-}	[27]aneN$_9$ ATP^{4-}	[30]aneN$_{10}$ ATP^{4-}	[33]aneN$_{11}$ ATP^{4-}	[36]aneN$_{12}$ ATP^{4-}
				(log K)					
L + 3H + A[a] = LH_3A	30.99(3)[b]	—	—	30.26(4)	—	—	—	—	—
L + 4H + A = LH_4A	38.70(1)	37.16(1)	37.48(1)	38.63(1)	39.35(1)	39.85(2)	40.39(3)	40.36(4)	—
L + 5H + A = LH_5A	43.92(2)	42.91(1)	43.13(1)	45.10(1)	47.09(1)	48.46(1)	49.43(1)	49.00(2)	48.89(1)
L + 6H + A = LH_6A	—	46.96(2)	47.92(1)	50.48(2)	53.37(1)	55.62(1)	57.67(1)	57.84(2)	57.34(2)
L + 7H + A = LH_7A	—	50.79(1)	51.96(1)	54.85(2)	58.17(1)	61.19(1)	64.46(1)	65.02(2)	64.57(1)
L + 8H + A = LH_8A	—	53.68(1)	54.91(1)	58.53(2)	61.99(1)	65.54(2)	69.75(1)	70.81(2)	70.51(1)
L + 9H + A = LH_9A	—	—	—	—	65.19(1)	69.20(2)	73.99(2)	75.45(2)	75.47(2)
L + 10H + A = $LH_{10}A$	—	—	—	—	—	72.25(2)	77.53(2)	79.35(2)	79.76(1)
L + 11H + A = $LH_{11}A$	—	—	—	—	—	—	80.46(2)	82.77(2)	83.57(1)
L + 12H + A = $LH_{12}A$	—	—	—	—	—	—	—	85.40(3)	86.62(1)
L + 13H + A = $LH_{13}A$	—	—	—	—	—	—	—	—	88.93(2)
LH_3 + A = LH_3A	2.47	—	—	2.59	—	—	—	—	—
LH_4 + A = LH_4A	5.91	3.07	3.39	4.54	3.74	3.84	3.58	3.47	—
LH_5 + A = LH_5A	8.92	4.99	5.31	7.28	6.93	6.09	4.83	4.02	3.53
LH_6 + A = LH_6A	—	7.00	7.96	10.52	9.79	9.03	7.82	6.39	4.16
LH_7 + A = LH_7A	—	8.87	10.04	12.93	11.89	11.37	10.77	9.06	5.73
LH_8 + A = LH_8A	—	—	—	—	13.81	13.41	13.04	11.27	7.40
LH_9 + A = LH_9A	—	—	—	—	—	15.24	15.31	13.16	8.78
LH_{10} + A = $LH_{10}A$	—	—	—	—	—	—	17.07	14.83	10.45
LH_{11} + A = $LH_{11}A$	—	—	—	—	—	—	—	16.58	11.93
LH_{12} + A = $LH_{12}A$	—	—	—	—	—	—	—	—	14.13
LH_k + HA = LH_kAH	—	—	—	10.37	10.78	11.95	13.76	12.97	10.20

Note. The constants of the systems ADP-[21]aneN$_7$ and AMP-[21]aneN$_7$ under the same conditions are also included.

[a] A represents AMP^{2-}, ADP^{3-}, and ATP^{4-}.

[b] The values in parentheses are standard deviations in the last significant figure. Charges have been omitted for clarity.

TABLE 3

Logarithms of the Stability Constants for the Systems PO_4^{3-}/[3k]aneN$_k$ (k = 7–12) in 0.15 mol dm^{-3} $NaClO_4$ at 298.15 K

Reaction	[21]aneN$_7$	[24]aneN$_8$	[27]aneN$_9$	[30]aneN$_{10}$	[33]aneN$_{11}$
		(log K)			
L + 4H + A = LH$_4$A[a]	—	40.81(8)[b]	41.53(5)	—	43.12(3)
L + 5H + A = LH$_5$A	48.63(1)	49.79(2)	50.15(3)	49.98(6)	51.64(4)
L + 6H + A = LH$_6$A	54.49(2)	56.73(3)	57.73(2)	57.96(5)	60.42(2)
L + 7H + A = LH$_7$A	59.19(1)	62.07(3)	63.77(2)	64.89(4)	67.98(2)
L + 8H + A = LH$_8$A	62.82(2)	65.75(3)	68.24(3)	70.12(5)	74.50(2)
L + 9H + A = LH$_9$A	—	68.18(4)	71.49(3)	74.47(3)	79.57(3)
L + 10H + A = LH$_{10}$A	—	—	74.00(4)	77.68(3)	83.39(3)
L + 11H + A = LH$_{11}$A	—	—	—	80.45(2)	86.47(3)
L + 12H + A = LH$_{12}$A	—	—	—	—	88.82(4)
LH$_4$ + A = LH$_4$A	—	5.20	5.50	—	6.23
LH$_5$ + A = LH$_5$A	10.81	9.63	7.75	5.39	6.66
LH$_6$ + A = LH$_6$A	14.53	13.15	11.10	8.13	8.97
LH$_7$ + A = LH$_7$A	17.27	15.78	13.91	11.22	12.02
LH$_8$ + A = LH$_8$A	—	17.57	16.07	13.43	14.97
LH$_9$ + A = LH$_9$A	—	—	17.52	15.81	17.29
LH$_{10}$ + A = LH$_{10}$A	—	—	—	17.23	18.88
LH$_{11}$ + A = LH$_{11}$A	—	—	—	—	20.28

[a] A represents PO_4^{3-}.

[b] The values in parentheses are standard deviations in the last significant figure. Charges have been omitted for clarity.

SUPERQUAD under our experimental conditions revealed predominantly 1 : 1 stoichiometries for all the species detected.

By examining the different values of stability constants, several main features can be readily noticed. For all the studied anions, the interaction with the macrocycle starts to be detectable for a minimum protonation of four, except for the systems $P_2O_7^{4-}$–[21]aneN$_7$, ATP–[21]aneN$_7$, and ATP–[18]aneN$_6$ for which just three protons are required on the macrocycle to make the interaction detectable. The highest pH value at which these interactions are appreciable is usually $\cong$ 9.

For a given macrocycle the strength of the interaction increases with its degree of protonation. For instance, the stability constants for the interaction between $P_2O_7^{4-}$ and [21]aneN$_7$ vary from log K = 2.74(3) for the triprotonated macrocycle to log K = 16.49(2) for the macrocycle in its heptaprotonated form, while in the case of ATP the constants for the same degrees of protonation vary from 2.59(4) to 12.93(2) (see Tables 2, 3, and 4 and Figs. 1a–1c).

For a determined protonation degree of both reagents, anion and macrocycle, a decrease in stability occurs as the macrocyclic size increases, which may be attributed to a decrease in charge density and possibly an increase in macrocyclic flexibility. The cyclic nature of these polyamines does allow for the formation of polyammonium cations having high charge density, and must be the reason why macrocyclic ligands interact more strongly with anions than do their noncyclic

TABLE 4

Logarithms of the Stability Constants for the Systems $P_2O_7^{4-}$/[3*k*]aneN$_k$ (*k* = 7–12) in 0.15 mol dm^{-3} $NaClO_4$ at 298.15 K

Reaction	[21]aneN$_7$	[24]aneN$_8$	[27]aneN$_9$	[30]aneN$_{10}$	[33]aneN$_{11}$
		(log *K*)			
L + 3H + A = LH$_3$A[a]	30.41(3)[b]	—	—	—	—
L + 4H + A = LH$_4$A	39.74(1)	40.51(1)	40.84(2)	40.50(3)	40.61(2)
L + 5H + A = LH$_5$A	47.11(1)	48.54(3)	49.94(1)	49.95(1)	49.71(1)
L + 6H + A = LH$_6$A	53.31(1)	55.14(6)	57.49(1)	58.16(1)	58.68(1)
L + 7H + A = LH$_7$A	58.41(1)	60.43(8)	63.58(1)	65.03(1)	66.21(1)
L + 8H + A = LH$_8$A	62.30(2)	64.3(1)	68.24(2)	70.74(1)	72.83(1)
L + 9H + A = LH$_9$A	—	67.3(1)	71.75(2)	75.14(2)	78.39(1)
L + 10H + A = LH$_{10}$A	—	—	74.26(4)	79.08(2)	82.98(1)
L + 11H + A = LH$_{11}$A	—	—	—	81.61(2)	86.84(1)
L + 12H + A = LH$_{12}$A	—	—	—	—	89.53(1)
LH$_3$ + A = LH$_3$A	2.74	—	—	—	—
LH$_4$ + A = LH$_4$A	5.65	4.90	4.81	3.70	3.71
LH$_5$ + A = LH$_5$A	9.29	8.39	7.54	5.36	4.73
LH$_6$ + A = LH$_6$A	13.35	11.56	10.87	8.33	7.23
LH$_7$ + A = LH$_7$A	16.49	14.14	13.72	11.36	10.25
LH$_8$ + A = LH$_8$A	—	16.12	16.07	14.05	13.30
LH$_9$ + A = LH$_9$A	—	—	17.78	16.48	16.10
LH$_{10}$ + A = LH$_{10}$A	—	—	—	18.63	18.46
LH$_{11}$ + A = LH$_{11}$A	—	—	—	—	20.05

[a] A represents $P_2O_7^{4-}$ anion.

[b] The values in parentheses are standard deviations in the last significant figure. Charges have been omitted for clarity.

counterparts (*1*). Nevertheless, hydrogen bonding plays a crucial role in these kinds of interactions; for example, ATP fails to interact with the tetrapositively charged macrocycle 1,1,4,4,7,7,10,10-octamethyl-1,4,7,10-tetraazacyclododecane, in which hydrogen bonding has been prevented by quaternization of the amine groups (*15*).

An exception to the above trend is observed in the system PO_4^{3-}–[33]aneN$_{11}$ for which an increase in stability with respect to PO_4^{3-}–[30]aneN$_{10}$ is observed (see Table 3, Fig. 1b). It is difficult to establish the reason for this increase without any structural information. Nevertheless, it could suggest a more favorable incorporation of the anion into the macrocyclic cavity. This possibility gains credence as a result of the recent crystal structure of the compound [(PdCl$_4$)(H$_{10}$[30]aneN$_{10}$)](PdCl$_4$)$_2$Cl$_4$ in which a $[PdCl_4]^{2-}$ anion is snuggly placed in the center of the decaprotonated macrocycle, forming several short NH···Cl hydrogen bonds (*23*).

Crystal Structure of [21]aneN$_7$

Final fractional coordinates are given in Table 5. The 21-membered macrocycle crystallized as the tetrachloride salt with one molecule of water. Bond distances and angles are as anticipated (Tables 6 and 7, respectively).

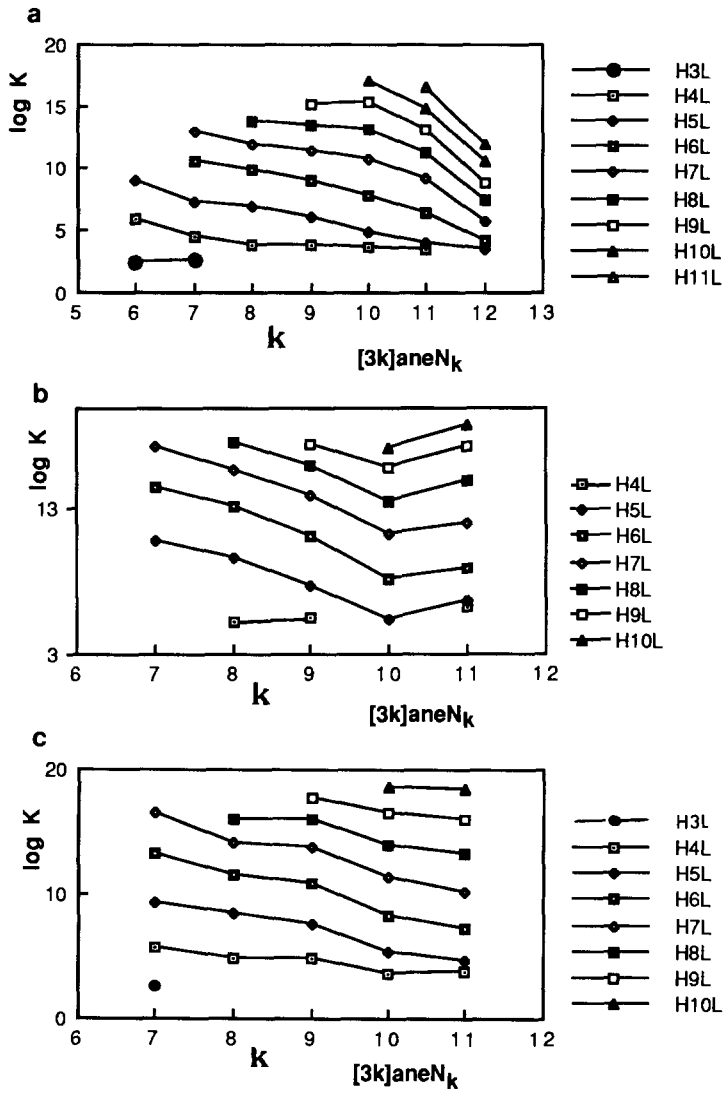

FIG. 1. (a) Variation of the succesive stability constants of ATP-[3k]aneN$_k$ (k = 6–12) systems with the dimension of the macrocycle. (b) Variation of the successive stability constants of PO_4^{3-}-[3k]aneN$_k$ (k = 7–11) systems with the dimension of the macrocycle. (c) Variation of the succesive stability constants of $P_2O_7^{4-}$-[3k]aneN$_k$ (k = 7–11) systems with the dimension of the macrocycle.

The macrocycle itself is a boat-shaped ellipsoid (Figs. 2 and 3), as has been found for several other polyaaza macrocycles (*24, 25*). Two of the neutral amines (determined by examining electron density maps for amine hydrogens) are found at the ends of the major axis of the ellipse. Interestingly, in several other structures, it has been observed that either ether oxygen atoms (with two lone pairs of electrons) (*24, 25*) or neutral amine nitrogen atoms (with one lone pair) (*26, 27*) occupy these sites.

TABLE 5

Fractional Positional Parameters for [21]aneN$_7$.

Atom	*x*	*y*	*z*
Cl(1)	0.1949(2)	0.2742	0.2052(1)
Cl(2)	0.413(2)	0.0139(1)	0.5020(2)
Cl(3)	0.6503(2)	0.4074(1)	0.9262(2)
Cl(4)	0.7292(2)	0.1423(1)	0.9358(2)
O(1)	0.7762(7)	0.2798(3)	0.7377(6)
N(1)	0.5642(7)	0.1195(3)	0.3030(8)
N(4)	0.3103(7)	0.1437(3)	1.0093(7)
N(7)	0.2029(9)	0.2520(3)	0.7775(6)
N(10)	0.2300(6)	0.3895(3)	0.9149(6)
N(13)	0.3691(6)	0.4816(3)	1.1935(6)
N(16)	0.6939(6)	0.4079(3)	1.3315(7)
N(19)	0.8178(6)	0.2237(3)	1.2636(6)
C(2)	0.368(1)	0.1069(4)	1.2976(8)
C(3)	0.277(1)	0.0906(4)	1.127(1)
C(5)	0.226(1)	0.1309(4)	0.8407(8)
C(6)	0.2622(9)	0.1863(4)	0.7295(7)
C(8)	0.2579(9)	0.3097(4)	0.6881(7)
C(9)	0.177(1)	0.3752(4)	0.7368(8)
C(11)	0.1321(8)	0.4489(4)	0.9668(9)
C(12)	0.1781(8)	0.4608(3)	1.1449(8)
C(14)	0.4378(9)	0.4799(3)	1.3688(8)
C(15)	0.5342(8)	0.4129(4)	1.4158(8)
C(17)	0.7946(8)	0.3430(3)	1.3542(8)
C(18)	0.7035(7)	0.2863(3)	1.2498(7)

Torsion angles around the ring are given in Table 8. The average C–C–N–C angles around N(1), N(4), N(7), and N(10) are consistently near the antiperiplanar (*trans*) configuration of 180° (average of 172.5°). The carbons leading to N(13) and N(16) are a mixture of the antiperiplanar and synclinal (gauche) conformation depending on the direction of approach. N(19) is more appropriately described as being in the gauche conformation (average of 67.6 compared to an ideal 60°).

There are a number of hydrogen bonding interactions among the water molecule, chlorides, and macrocycle (Table 9), although neither the water nor the chlorides are incorporated within the macrocycle. Specifically, Cl(1) interacts with N(4), N(10), and N(19); Cl(3) interacts with N(10) and O(1); and Cl(4) interacts with N(19) and O(1). There are no hydrogen bonding interactions between the nitrogens of the macrocycle.

Perhaps one of the most important aspects of the molecular structure is the size of the cavity. One way in which to describe overall size is by determining the lengths of the axes of the average ellipsoid of its structure. For [21]aneN$_7$ the average ellipsoid is 7.653 × 6.725 Å. As anticipated, the macrocycle is smaller than that found for the extensively studied [24]N$_6$O$_2$ (*1–3*), which is even more elliptical (10.005 × 6.714 Å) (*24*). Of significance in this respect are the results of

TABLE 6

Interatomic Distances for [21]aneN$_7$

Atoms	Distance (Å)	Atoms	Distance (Å)
N(1)–C(2)	1.481(9)	N(16)–C(17)	1.466(8)
N(1)–C(21)	1.434(8)	N(19)–C(18)	1.481(7)
N(4)–C(3)	1.48(1)	N(19)–C(20)	1.490(8)
N(4)–C(5)	1.459(8)	C(2)–C(3)	1.50(1)
N(7)–C(6)	1.43(1)	C(5)–C(6)	1.48(1)
N(7)–C(8)	1.45(1)	C(8)–C(9)	1.50(1)
N(10)–C(9)	1.497(8)	C(11)–C(12)	1.49(1)
N(10)–C(11)	1.475(9)	C(14)–C(15)	1.508(9)
N(13)–C(12)	1.469(8)	C(17)–C(18)	1.493(8)
N(13)–C(14)	1.463(9)	C(20)–C(21)	1.509(9)
N(16)–C(15)	1.495(8)		

energy minimization studies for the latter macrocycle, which indicate that the preferred orientation of the nucleotide with respect to the macrocycle is along the minor elliptical axis (*24*), which, for the two macrocycles, is almost identical (6.714 and 6.725 Å). This may be a critical factor in the catalytic efficiency of macrocycles.

The results of several recent crystal structures are also of interest: one of [30]aneN$_{10}$ with an associated hexacyanocobaltate(III) anion (*26*) and two of protonated forms of [18]aneN$_6$ (hexacyclen) (*27, 28*). These structures are elliptical, but not boat-shaped. Somewhat surprising is the finding that while the major axes vary significantly with macrocyclic size, the minor axes are all very similar (Table 10). Thus, while the major axes range from 7.647 to 15.486 Å for fully protonated [18]aneN$_6$ (*28*), to octaprotonated [30]aneN$_{10}$ (*26*), respectively, the minor axes only vary from 6.212 to 6.873 Å for tetraprotonated [18]aneN$_6^{27}$ to [30]aneN$_{10}^{26}$. So while [18]aneN$_6$ is smaller by ~0.5 Å than the efficient 21-membered system, the

TABLE 7

Bond Angles for [21]aneN$_7$ (deg)

Atoms	Angle (deg)	Atoms	Angle (deg)
C(2)–N(1)–C(21)	113.8(5)	N(7)–C(8)–C(9)	110.8(5)
C(3)–N(4)–C(5)	115.3(5)	N(10)–C(9)–C(8)	112.5(6)
C(6)–N(7)–C(8)	114.6(5)	N(10)–C(11)–C(12)	112.3(5)
C(9)–N(10)–C(11)	112.5(5)	N(13)–C(12)–C(11)	111.0(5)
C(12)–N(13)–C(14)	114.8(5)	N(13)–C(14)–C(15)	110.2(5)
C(15)–N(16)–C(17)	115.5(5)	N(16)–C(15)–C(14)	108.5(5)
C(18)–N(19)–C(20)	116.7(5)	N(16)–C(17)–C(18)	113.1(4)
N(1)–C(2)–C(3)	109.9(6)	N(19)–C(18)–C(17)	111.5(4)
N(4)–C(3)–C(2)	112.6(6)	N(19)–C(20)–C(21)	112.9(5)
N(4)–C(5)–C(6)	112.7(5)	N(1)–C(21)–C(20)	109.4(5)
N(7)–C(6)–C(5)	111.9(5)		

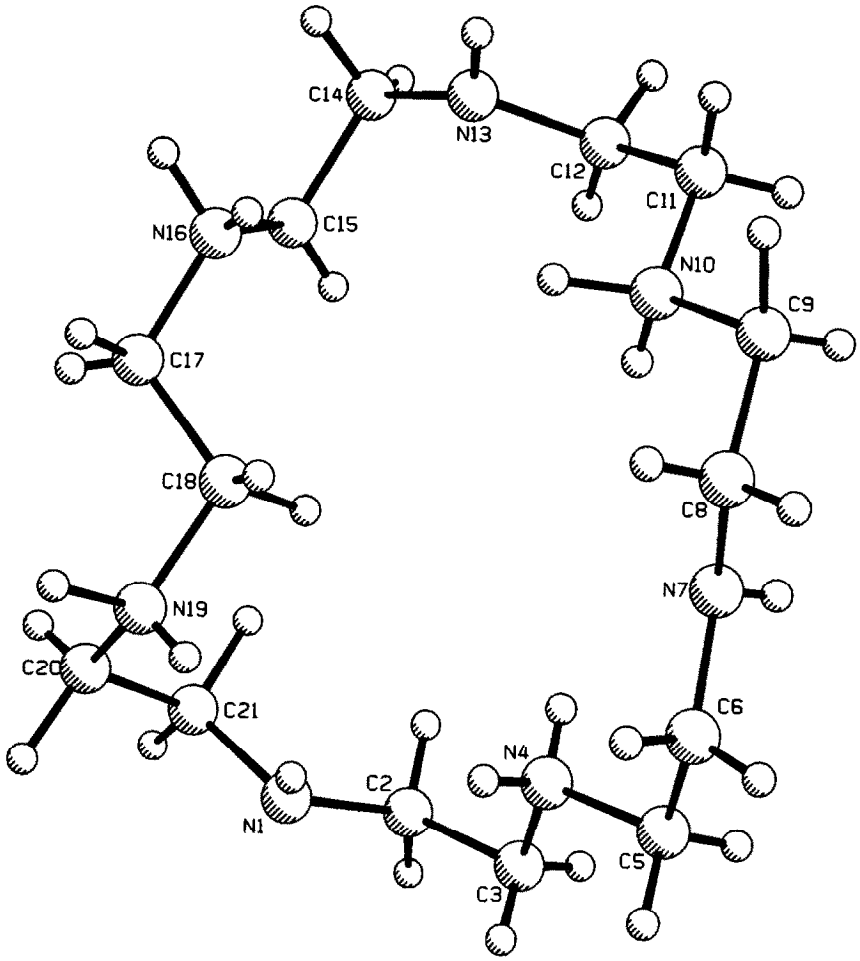

FIG. 2. Overhead perspective view of [21]aneN$_7$.

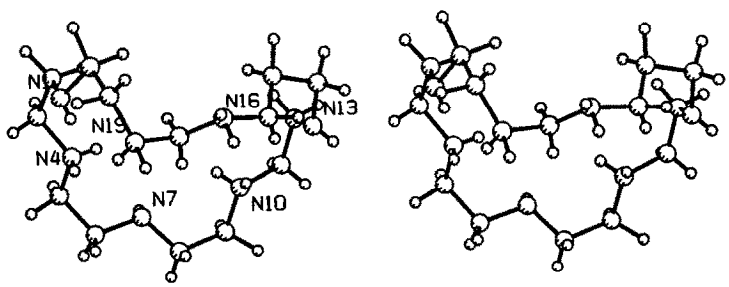

FIG. 3. Side stereo view of [21]aneN$_7$.

TABLE 8

Torsion Angles for [21]aneN$_4$

Atoms	Angle (deg)	Atoms	Angle (deg)
N(1)–C(2)–C(3)–N(4)	−52.9(9)	C(5)–C(6)–N(7)–C(8)	171.5(6)
N(1)–C(21)–C(20)–N(19)	52.8(7)	C(6)–N(7)–C(8)–C(9)	175.3(6)
N(4)–C(5)–C(6)–N(7)	−57.1(8)	C(8)–C(9)–N(10)–C(11)	−172.5(6)
N(7)–C(8)–C(9)–N(10)	58.1(7)	C(9)–N(10)–C(11)–C(12)	177.2(6)
N(10)–C(11)–C(12)–N(13)	66.3(7)	C(11)–C(12)–N(13)–C(14)	−167.2(6)
N(13)–C(14)–C(15)–N(16)	62.2(7)	C(12)–N(13)–C(14)–C(15)	95.6(6)
N(16)–C(17)–C(18)–N(19)	174.3(5)	C(14)–C(15)–N(16)–C(17)	−175.4(5)
C(2)–N(1)–C(21)–C(20)	−164.4(5)	C(15)–N(16)–C(17)–C(18)	78.6(7)
C(2)–C(3)–N(4)–C(5)	179.9(7)	C(17)–C(18)–N(19)–C(20)	73.7(7)
C(3)–N(4)–C(5)–C(6)	179.2(6)	C(18)–N(19)–C(20)–C(21)	61.2(7)
C(3)–C(2)–N(1)–C(21)	160.7(6)		

30-membered ring is only a little larger (<0.2 Å) along the minor axis. Nonetheless, while macrocyclic size may be a major factor in the catalytic aptitude of these macrocycles, it is clearly not the only consideration. Based on these structural results larger rings potentially are suitably sized, at least along the minor axis in the solid state, and should certainly be flexible enough to accommodate ATP.

ATPase Kinetic Studies

The ability of the present series of polyammonium macrocycles to catalyze the cleavage of ATP was examined. Loss of ATP was monitored by HPLC and, in several instances, by ^{31}P NMR spectroscopy. Measurements were performed at pH 3 and 7.

Since the species resulting from ATP hydrolysis are ADP, AMP, phosphate, and sometimes pyrophosphate (*2*), it was of interest to examine if inhibiting actions could be developed by the relevant anions. If such interactions were to occur, they could lead to erroneous conclusions about the apparent first order rate constants for the dephosphorylation of ATP. When a comparison between the abilities of the different anions to bind to these polyammonium macrocyclic cations is made for

TABLE 9

Hydrogen Bonding Interactions for [21]aneN$_7$ (Å)

B···H–A	B···A	B···H–A	B···A
Cl(1)···H(4A)–N(4)	3.224(6)	Cl(3)···H(16B)–N(16)	3.347(6)
Cl(1)···H(10A)–N(10)	3.352(6)	Cl(4)···H(23)–O(1)	3.201(6)
Cl(1)···H(19B)–N(19)	3.105(5)	Cl(4)···H(1)–N(1)	3.538(7)
Cl(2)···H(16A)–N(16)	3.021(5)	Cl(4)···H(4B)–N(4)	3.297(6)
Cl(3)···H(22)–O(1)	3.176(6)	Cl(4)···H(19A)–N(19)	3.133(6)
Cl(3)···H(10B)–N(10)	3.144(5)	O(1)···H(7)–N(7)	3.192(8)

TABLE 10

Major and Minor Axes from Crystallographic Data for the Average Ellipsoid of Polyammonium Macrocycles Ranging in Size from 18 to 30 Ring Atoms[a]

Macrocycle	Major axis (Å)	Minor axis (Å)
[18]aneN$_6$ · 4H	7.682	6.212
[18]aneN$_6$ · 6H	7.647	6.236
[21]aneN$_7$ · 4H	7.653	6.725
[24]aneN$_6$O$_2$ · 6H	10.005	6.714
[30]aneN$_{10}$ · 8H · Co(CN)$_6$	15.486	6.873

[a] The ellipsoid which represents the best fit on the image projected on the least-squares plane of the macrocycles.

a determined protonation state of the macrocycle, the following trend for the equilibrium constants is observed: $PO_4^{3-} > P_2O_7^{4-} > ATP^{4-} > ADP^{3-} > AMP^{2-}$. This trend can again be explained in terms of charge density and hydrogen bonding. Furthermore, it was found that anions with a charge less than -3 showed little interaction with the macrocycles. In order to ascertain whether inhibition by the products is occurring as the reaction proceeds, however, the protonation constants

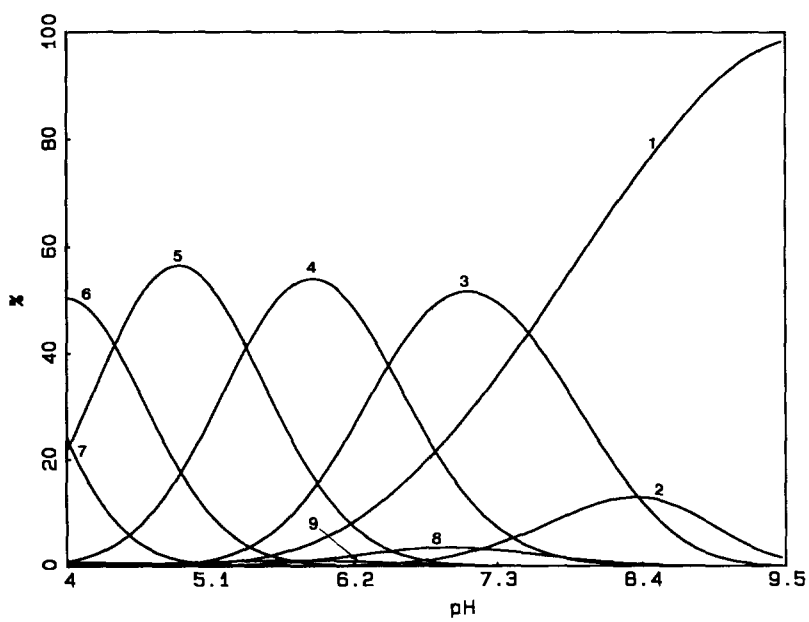

FIG. 4. Distribution diagram for the species present in solution for a mixture ATP : PO_4^{3-} : [21]aneN$_7$ (1 : 1 : 1) with initial concentrations 10^{-3} mol dm^{-3} (1) ATP^{4-}, (2) [H$_3$([21]aneN$_7$)-ATP]$^-$, (3) [H$_4$([21]aneN$_7$)ATP], (4) [H$_5$([21]aneN$_7$)ATP]$^+$, (5) [H$_6$([21]aneN$_7$)ATP]$^{2+}$, (6) [H$_7$([21]aneN$_7$)ATP]$^{3+}$, (7) [H$_8$([21]aneN$_7$)ATP]$^{4+}$, (8) [H$_5$([21]aneN$_7$)PO$_4$]$^{2+}$, (9) [H$_6$([21]aneN$_7$)PO$_4$]$^{3+}$.

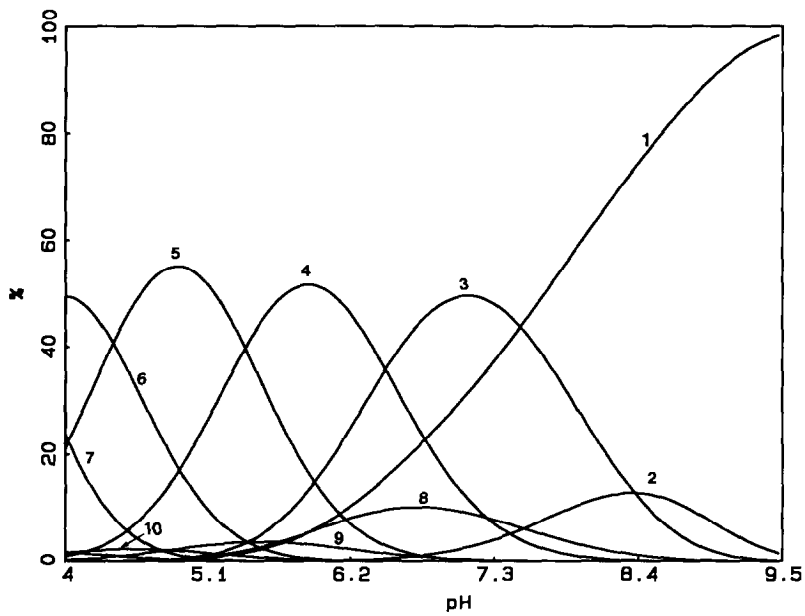

FIG. 5. Distribution diagram for the species present in solution for a mixture ATP : ADP : [21]aneN$_7$ (1 : 1 : 1) with initial concentrations 10^{-3} mol dm^{-3}. (1) ATP^{4-}, (2) $[H_3([21]aneN_7)ATP]^-$, (3) $[H_4([21]aneN_7)ATP]$, (4) $[H_5([21]aneN_7)ATP]^+$, (5) $[H_6([21]aneN_7)ATP]^{2+}$, (6) $[H_7([21]aneN_7)ATP]^{3+}$, (7) $[H_8([21]aneN_7)ATP]^{4+}$, (8) $[H_4([21]aneN_7)ADP]^+$, (9) $[H_5([21]aneN_7)ADP]^{2+}$, (10) $[H_6([21]aneN_7)ADP]^{3+}$.

of the different anions studied (*16*) must be taken into account; i.e., the maximally charged species PO_4^{3-}, $P_2O_7^{4-}$, ATP^{4-}, ADP^{3-}, and AMP^{2-} predominate at different pH values. A distribution diagram for the species present in solution for a mixture ATP : PO_4^{3-} : [21]aneN$_7$ (all three components in concentrations of 10^{-3} mol dm^{-3}) shows that ATP complexes are the main species in solution (Fig. 4). In fact, under these conditions, only 5% of the PO_4^{3-} species $[H_5([21]aneN_7)PO_4]^{2+}$ is formed at pH 7, and the protonated forms of phosphate (HPO_4^{2-} and $H_2PO_4^-$) are the species competing with ATP^{4-}, $HATP^{3-}$, and H_2ATP^{2-} for coordination to the macrocycle. This situation exists between pHs 2.5 and 9.5. The distribution diagrams for mixtures ATP : ADP : [21]aneN$_7$ and ATP : AMP : [21]aneN$_7$ with concentrations 10^{-3} mol dm^{-3} in each (Figs. 5 and 6) show that also in these cases the ATP–macrocycle complexes predominate, reaching $[H_4([21]aneN_7)ADP]^+$ (Fig. 5) and $[H_4([21]aneN_7)AMP]^{2+}$ (Fig. 6) for a maximum of just 10 and 5%, respectively. These results indicate that at least at this concentration level, ATP hydrolysis induced by large polyazacycloalkanes is free, for the major part, of inhibiting agents generated by its own hydrolysis. In fact, the only species that could exert a real inhibiting effect would be pyrophosphate (see Fig. 7), but pyrophosphate is not formed under these experimental conditions. On the other hand, in the case of acetylphosphate hydrolysis as catalyzed by polyammonium macrocycles, it has

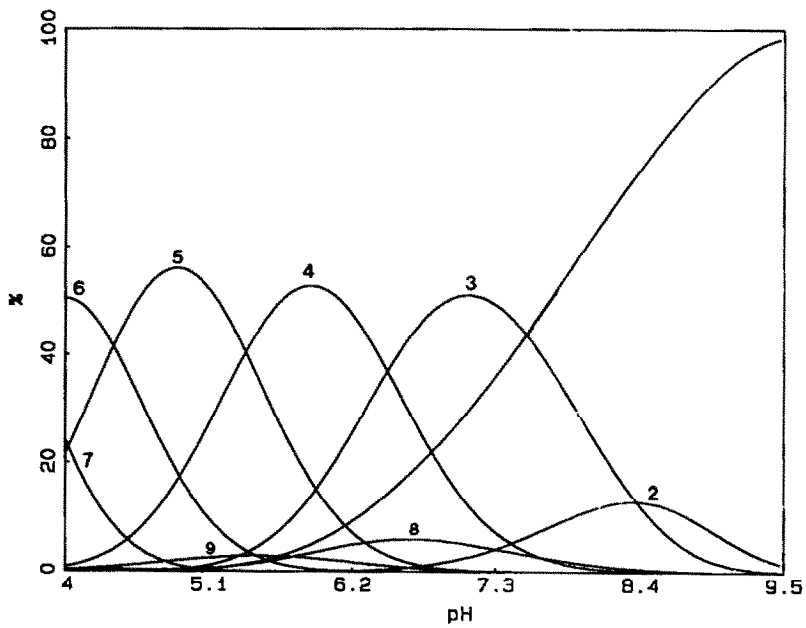

FIG. 6. Distribution diagram for the species present in solution for a mixture ATP : AMP : [21]aneN$_7$ (1 : 1 : 1) with initial concentrations 10^{-3} mol dm^{-3} (1) ATP^{4-}, (2) [H$_3$([21]aneN$_7$)ATP]$^-$, (3) [H$_4$([21]aneN$_7$)ATP], (4) [H$_5$([21]aneN$_7$)ATP]$^+$, (5) [H$_6$([21]aneN$_7$)ATP]$^{2+}$, (6) [H$_7$([21]aneN$_7$)ATP]$^{3+}$, (7) [H$_8$([21]aneN$_7$)ATP]$^{4+}$, (8) [H$_4$([21]aneN$_7$)AMP]$^{2+}$, (9) [H$_5$([21]aneN$_7$)AMP]$^{3+}$.

been found that the resulting monohydrogenphosphate effectively inhibits the dephosphorylation process (*2d*).

The rates of dephosphorylation were found to be dependent on concentration, with up to almost 10-fold increases observed when progressing from 10^{-5} mol dm^{-3} to 10^{-2} mol dm^{-3} concentrations of both ATP and macrocycle. This can be explained by the fact that the lower concentrations used in the HPLC measurements are approaching that of K_d for the complex, so that an appreciable amount of uncomplexed ATP exists in solution. An enzyme kinetic analysis of the reaction with [24]aneN$_6$O$_2$ and [18]aneN$_6$ has indicated that preassociation of the substrate and catalyst in a reactive Michaelis-type complex occurs, and is critical to the catalytic sequence (*3a*). This finding is also in agreement with the observed faster rates of hydrolysis at lower pH (vide infra), where there is a higher degree of complex formation.

At pH 3 the fastest rate for ATP hydrolysis was observed in the presence of [21]aneN$_7$ (k = 0.029 min^{-1} at 20°C, Table 11). At higher temperatures the rates for this macrocycle were too fast to be monitored using HPLC and NMR techniques. All of the other macrocycles were considerably slower, with [24]aneN$_8$ being the fastest of these at k = 0.0045 min^{-1} at 40°C. The rates observed in the presence of the four larger macrocycles ranged from factors of 3 to 7 slower than [24]aneN$_8$. Results from [18]aneN$_6$ have been previously reported (*1a*). Using lower concentrations and HPLC techniques, the rate was also found to be ex-

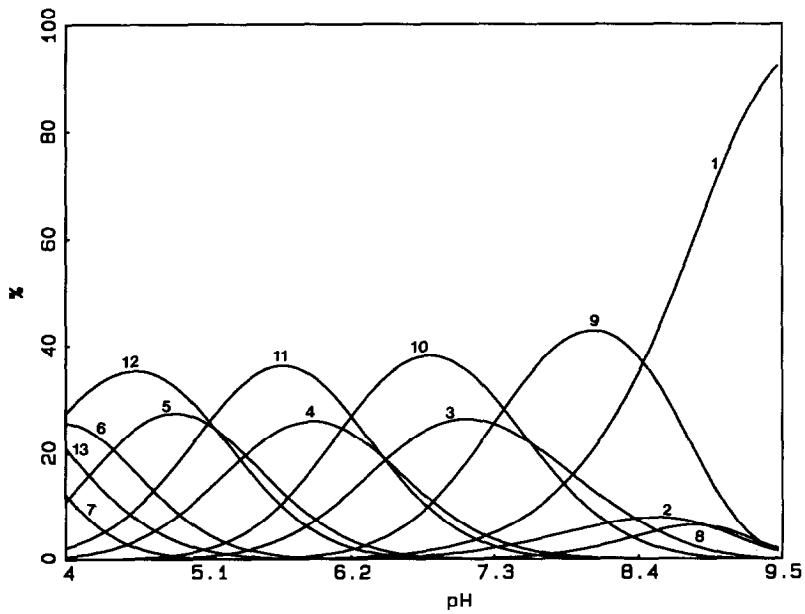

FIG. 7. Distribution diagram for the species present in solution for a mixture ATP: $P_2O_7^{4-}$: [21]aneN$_7$ (1 : 1 : 1) with initial concentrations 10^{-3} mol dm^{-3}. (1) ATP^{4-}, (2) [H_3([21]aneN$_7$)ATP]$^-$, (3) [H_4([21]aneN$_7$)ATP], (4) [H_5([21]aneN$_7$)ATP]$^+$, (5) [H_6([21]aneN$_7$)ATP]$^{2+}$, (6) [H_7([21]aneN$_7$)ATP]$^{3+}$, (7) [H_8([21]aneN$_7$)ATP]$^{4+}$, (8) [H_5([21]aneN$_7$)P_2O_7]$^-$, (9) [H_4([21]aneN$_7$)P_2O_7], (10) [H_5([21]aneN$_7$)P_2O_7]$^+$, (11) [H_6([21]aneN$_7$)P_2O_7]$^{2+}$, (12) [H_7([21]aneN$_7$)P_2O_7]$^{3+}$, (13) [H_8([21]aneN$_7$)P_2O_7]$^{4+}$.

tremely slow. Hence, 21- and 24-membered rings seem to display the maximum efficiency. It should also be noted that a small amount of phosphoramidate intermediate could be observed in the NMR spectrum at pH 4 for [21]aneN$_7$. General acid catalysis could play a major role in facilitating the reaction at lower pH, with proton transfer from one of the protonated amines to the P–O–P oxygen, potentially resulting in an assist to P–O bond cleavage:

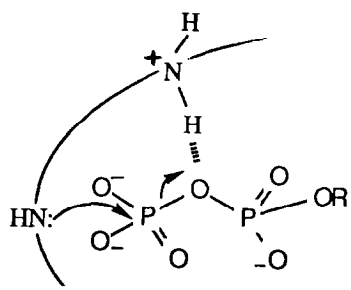

At pH 7 the rates were considerably slower than at pH 3. This finding can be partly attributed to the lesser degree of protonation of the macrocycle, which results in lower affinity and lessened participation of general acid catalysis. Studies

TABLE 11

Rates of Hydrolysis of ATP in the Presence of Polyazamacrocycles[a]

Macrocycle	pH (±0.1)	Concn. (M)	Temp.(°C)	Rate (min^{-1}, $\times 10^3$)
[18]aneN$_6$	3.0	10^{-3}*	80	4.5
	7.0	10^{-3}*	80	1.8
[21]aneN$_7$	3.0	10^{-5}	20	29
	7.0	10^{-5}	70	8.7
	7.0	10^{-3}	70	53
	7.0	10^{-2}	70	104
	7.0	10^{-5}	25	0.18
[24]aneN$_8$	3.0	10^{-5}	40	4.5
	3.0	10^{-5}	70	110[b]
	7.0	10^{-5}	70	4.0
	7.0	10^{-3}	70	7.0
	7.0	10^{-2}	70	14
	7.0	10^{-5}	25	0.031
[27]aneN$_9$	3.0	10^{-5}	70	18
	3.0	10^{-5}	40	0.65
	7.0	10^{-5}	70	1.2
	7.0	10^{-3}	70	2.8
	7.0	10^{-2}	70	7.8
	7.0	10^{-5}	25	0.017
[30]aneN$_{10}$	3.0	10^{-5}	40	1.1
	3.0	10^{-5}	70	13
	7.0	10^{-5}	70	0.77
	7.0	10^{-3}	70	2.2
	7.0	10^{-5}	25	0.0083
[33]aneN$_{11}$	3.0	10^{-5}	40	0.86
	3.0	10^{-5}	70	8.4
	7.0	10^{-5}	70	0.54
	7.0	10^{-3}	70	1.4
	7.0	10^{-5}	25	0.011
[36]aneN$_{12}$	3.0	10^{-5}	70	24
	3.0	10^{-5}	40	1.4
	7.0	10^{-5}	70	0.63
	7.0	10^{-3}	70	1.3
	7.0	10^{-5}	25	0.0038

[a] Rates were the same at lower concentrations and the reactions were exceedingly slow even at 70°C.

[b] Approximate value only, due to rapid rate.

were done at 25°C, to correlate with the temperature at which the thermodynamic studies were performed, and at 70°C, where the reactions proceed at reasonably rapid rates. At both temperatures [21]aneN$_7$ exhibited the fastest rates. At 0.02 mol dm^{-3} concentrations and 70°C, the 21-membered macrocycle was over seven times faster (k = 0.104 min^{-1}) than the next fastest, [24]aneN$_8$ (k = 0.014 min^{-1}). Again dephosphorylation in the presence of the larger macrocycles as well as [18]aneN$_6$ appeared to be considerably slower.

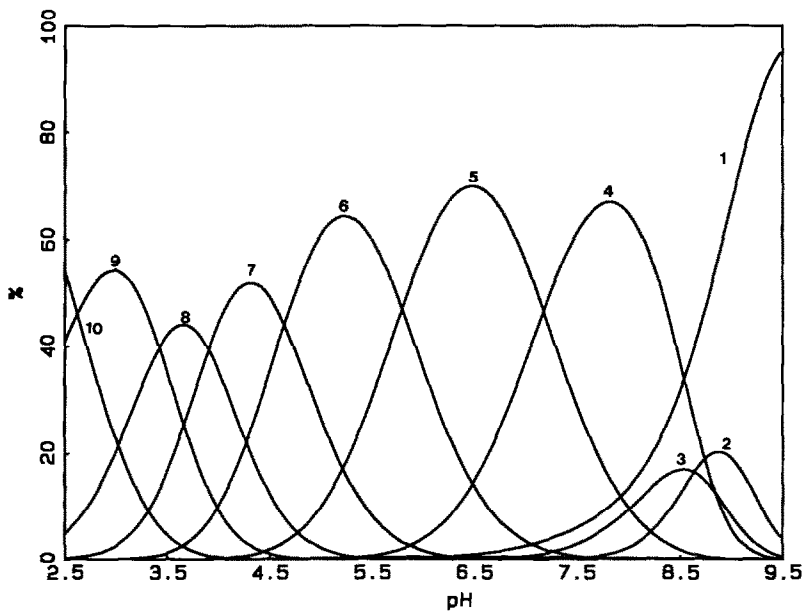

FIG. 8. Distribution diagram for the species present in solution for the system ATP : [33]aneN$_{11}$ with initial concentrations for all 10^{-3} mol dm^{-3}. (1) ATP^{4-}, (2) [H$_4$([33]aneN$_{11}$)ATP], (3) [H$_5$([33]aneN$_{11}$)-ATP]$^+$, (4) [H$_6$([33]aneN$_{11}$)ATP]$^{2+}$, (5) [H$_7$([33]aneN$_{11}$)ATP]$^{3+}$, (6) [H$_8$([33]aneN$_{11}$)ATP]$^{4+}$, (7) [H$_9$([33]aneN$_{11}$)ATP]$^{5+}$, (8) [H$_{10}$([33]aneN$_{11}$)ATP]$^{6+}$, (9) [H$_{11}$([33]aneN$_7$)ATP]$^{7+}$, (10) [H$_{12}$([33]aneN$_{11}$)ATP]$^{8+}$.

The 21-membered [21]aneN$_7$ has proved to be the best catalyst of ATP hydrolysis of the macrocycles studied and is especially efficient at lower pHs. Several reasons could be put forward to explain this trend. One aspect involves the formation of a high affinity complex between the nucleotide and the macrocycle. The first step in the hydrolytic pathway is the formation of an ATP–macrocycle complex, which is required for the dephosphorylation (*3a*); [21]aneN$_7$ forms a highly stable complex. While this association is important, the extent of interaction cannot be the only critical aspect, since [18]aneN$_6$ interacts more strongly with ATP than [21]aneN$_7$, but produces lower rates. Also, consideration of the K_s's of the species involved at pH 7 leads to puzzling results when the degree of protonation is taken into account if complex formation is the only critical factor, since at a given pH, the K_s for the larger macrocycles exceeds that of [21]aneN$_7$. For instance, for ATP–[33]aneN$_{11}$, the species present in solution at pH 7 are [H$_6$([33]aneN$_{11}$)-ATP]$^{2+}$ and [H$_7$([33]aneN$_{11}$)ATP]$^{3+}$ (Fig. 8) with log K_s of 6.39 and 9.06 respectively, while in the case of ATP-[21]aneN$_7$ the species at the same pH value would be [H$_4$([21]aneN$_7$)ATP] and [H$_5$([21]aneN$_7$)ATP]$^+$ with considerably lower stability constants (4.54 and 7.28, respectively; Fig. 9). Despite this fact, [21]aneN$_7$ catalyzes, at the same pH, dephosphorylation at a much higher rate than [33]aneN$_{11}$.

A second factor associated with the catalytic aptitude of the macrocycles could

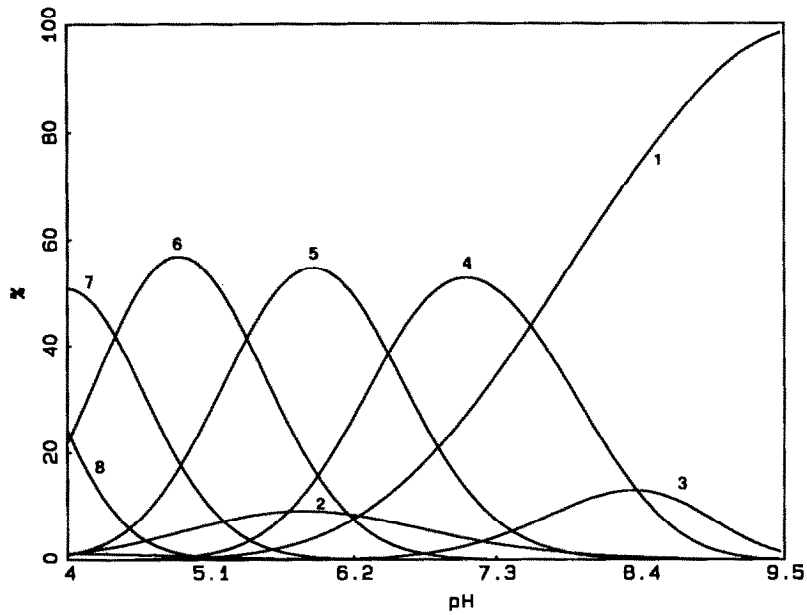

FIG. 9. Distribution diagram for the species present in solution for the system ATP : [21]aneN$_7$ (1 : 1) with initial concentrations 10^{-3} mol dm^{-3}. (1) ATP^{4-}, (2) $HATP^{3-}$, (3) $[H_3([21]aneN_7)ATP]^-$, (4) $[H_4([21]aneN_7)ATP]$, (5) $[H_5([21]aneN_7)ATP]^+$, (6) $[H_6([21]aneN_7)ATP]^{2+}$, (7) $[H_7([21]aneN_7)ATP]^{3+}$, (8) $[H_8([21]aneN_7)ATP]^{4+}$.

be the net macrocyclic–nucleotide complex charge. Of note is that at pH 7, a neutral complex is formed only for [21]aneN$_7$. All of the other macrocycles with ring sizes greater than 24 are involved in di- or tripositively charged complexes. If, as suspected based on prior studies (*1–3*), a covalent phosphoramidate intermediate is involved in these reactions, the nucleophilicity of the macrocyclic amines could be critical. Increased positive charge will tend to decrease the nucleophilicity of the unprotonated amines, hence resulting in rate decelerations. Therefore, if a covalent intermediate is a major pathway in the reaction sequence, the complexes with the lowest overall positive charges should be more efficient catalysts. This is the case for [21]aneN$_7$ at both pH 3 and 7.

CONCLUSIONS

The interaction of polyammonium macrocycles with phosphate species is extremely dependent on both ring size and degree of protonation, with K_s increasing with increasing degrees of protonation, but decreasing with increasing macrocyclic size. Both of these aspects play roles in the observed macrocyclic catalysis of the dephosphorylation of ATP. Of primary importance is the macrocyclic size, with the 21-membered [21]aneN$_7$ being the best catalyst at the pHs examined. The [24]aneN$_8$ was also reasonably effective. Rates are potentially related to the dis-

tance across the minor elliptical axis of the macrocycle, which is found to be almost identical for the most efficient 21- and 24-membered ring systems. Additionally, at pH 7, [21]aneN$_7$ is the only macrocycle to form a neutral complex with ATP, while all of the macrocycles larger than 24 ring members form di- and tripositively charged complexes. Hence, although the K_s's for the larger macrocycles at a given pH are larger, the positive charge serves to decrease the nucleophilicity of the amine lone pair of electrons. If the formation of the covalent phosphoramidate intermediate is an important pathway, this nucleophilicity of the amines will be a crucial aspect of the catalysis. At lower pHs, the rates are markedly increased, and this can be attributed to increased affinity of the more highly protonated macrocycle for the substrate, as well as an increased tendency for general acid catalysis of the P–O–P bond cleavage.

ACKNOWLEDGMENTS

Financial support from the Italian Ministeria della Pubblica Istruzione, the Spanish Comision Interministeria de Ciencia y Tecnologia (Projecto PB85-0190), and the National Institutes of Health (GM 33922) is gratefully acknowledged.

REFERENCES

1. (a) HOSSEINI, M. W., LEHN, J.-M., AND MERTES, M. P. (1983) *Helv. Chim. Acta* **66,** 2454–2466; (b) HOSSEINI, M. W., LEHN, J.-M., AND MERTES, M. P. (1985) *Helv. Chim. Acta* **68,** 818; (c) HOSSEINI, M. W., LEHN, J.-M., MAGGIORA, L., MERTES, K. B., AND MERTES, M. P. (1987) *J. Am. Chem. Soc.* **109,** 537–544; (d) BETHELL, R. C., LOWE, G., HOSSEINI, M. W., AND LEHN, J.-M. (1988) *Bioorg. Chem.* **16,** 418–428.
2. (a) YOHANNES, P. G., MERTES, M. P., AND MERTES, K. B. (1985) *J. Am. Chem. Soc.* **107,** 8288–8289; (b) YOHANNES, P. G., PLUTE, K. E., MERTES, M. P., AND MERTES, K. B. (1987) *Inorg. Chem.* **26,** 1751–1755; (c) HOSSEINI, M. W., AND LEHN, J.-M. (1985) *J. Chem. Soc. Chem. Commun.,* 1155–1157; (d) HOSSEINI, M. W., AND LEHN, J.-M. (1987) *J. Am. Chem. Soc.* **109,** 7047–7058; (e) BLACKBURN, G. M., THATCHER, G. R. J., HOSSEINI, M. W., AND LEHN, J.-M. (1987) *Tetrahedron Lett.* **28,** 2779–2782.
3. (a) JAHANSOUZ, H., JIANG, Z., HIMES, R. H., MERTES, M. P., AND MERTES, K. B. (1989) *J. Am. Chem. Soc.* **111,** 1409–1413; (b) JIANG, Z., CHALABI, P., MERTES, K. B., JAHANSOUZ, H., HIMES, R. H., AND MERTES, M. P. (1989) *Bioorg. Chem.* **17,** 313–329.
4. BIANCHI, A., MANGANI, S., MICHELONI, M., NANINI, V., ORIOLI, P., AND PAOLETTI, P. (1985) *Inorg. Chem.* **24,** 1182.
5. MICHELONI, M., PAOLETTI, P., AND BIANCHI, A. (1985) *Inorg. Chem.* **24,** 1182.
6. BENCINI, A., BIANCHI, A., GARCÍA-ESPAÑA, E., GIUSTI, M., MICHELONI, M., AND PAOLETTI, P. (1987) *Inorg. Chem.* **26,** 681.
7. BENCINI, A., BIANCHI, A., GARCÍA-ESPAÑA, E., GIUSTI, M., MANGANI, S., MICHELONI, M., ORIOLI, P., AND PAOLETTI, P. (1987) *Inorg. Chem.* **26,** 1243.
8. BENCINI, A., BIANCHI, A., GARCÍA-ESPAÑA, E., MICHELONI, M., AND PAOLETTI, P. (1988) *Inorg. Chem.* 1988, 27, 176.
9. MICHELONI, M., MAY, P. M., AND WILLIAMS, D. R. (1978) *J. Inorg. Nucl. Chem.* **40,** 1209.
10. MICHELONI, M., SABATINI, A., AND VACCA, A. (1977) *Inorg. Chim. Acta* **25,** 41.
11. BENKOVIC, S. J., AND SAMPSON, E. J. (1971) *J. Am. Chem. Soc.* **93,** 4009.

12. BIANCHI, A., BOLOGNI, L., DAPPORTO, P., MICHELONI, M., AND PAOLETTI, P. (1984) *Inorg. Chem.* **13,** 1201.
13. (a) GRAN, G. (1952) *Analyst (London)* **77,** 661; (b) Rossotti, F. J., and Rossotti, H. (1989). *J. Chem. Educ.* **28,** 1188.
14. BENCINI, A., BIANCHI, A., DAPPORTO, P., GARCÍA-ESPAÑA, E., MICHELONI, M., AND PAOLETTI, P. (1989) *Inorg.Chem.* **28,** 1188.
15. BIANCHI, A., MICHELONI, M., AND PAOLETTI, P. (1988) *Inorg. Chim. Acta* **151,** 269–272.
16. Protonation constants for ADP^{3-}, AMP^{2-}, PO_4^{3-}, and $P_2O_7^{4-}$ determined at 298.15 K and 0.15 mol dm^{-3} $NaClO_4$. ADP^{3-} : log B_1 = 6.16(1), log B_2 = 10.09(1); AMP^{2-} : log B_1 = 6.08(1), log B_2 = 9.91(1); PO_4^{3-} : log B_1 = 11.54(1), log B_2 = 18.26(1), log B_3 = 20.37(5); $P_2O_7^{4-}$: log B_1 = 8.138(3), log B_2 = 14.06(1), log B_3 = 16.00(5). B refers to the cumulative stability constants.
17. GANS, P., SABATINI, A., AND VACCA, A. (1985) *J. Chem. Soc. Dalton Trans.*, 1195.
18. Structure solution methods used MITHRIL (1984) *J. Appl. Crystallogr.* **17,** 42, and DIRDIF, Beurskens, P. T. (1985) Technical Report, Crystallography Laboratory, Toernooiveld, 6525 Ed Nijmegen, The Netherlands.
19. CROMER, D. T., AND WABER, J. T. (1974) *in* International Tables for X-Ray Crystallography, Vol. IV, Tables 2.2A and 2.3.1, Kynoch Press; Birmingham, England.
20. IBERS, J. A., AND HAMILTON, W. C. (1964) *Acta Crystallogr.* **17,** 781.
21. TEXSAN-TEXRAY Structure Analysis Package, Molecular Structure Corp. (1985).
22. DIETRICH, B., HOSSEINI, M. W., LEHN, J.-M., AND SESSIONS, R. B. (1981) *J. Am. Chem. Soc.* **103,** 1282.
23. BENCINI, A., BIANCHI, A., DAPPORTO, P., GARCÍA-ESPAÑA, E., MICHELONI, M., PAOLETTI, P., AND PAOLI, P. (1990) *J. Chem. Soc. Chem. Commun.* 1382–1384.
24. WANG, B., DEFFO, T., AND MERTES, K. B., submitted for publication.
25. QIAN, L., SUN, Z., GAO, J., MOVASSAGH, B., LU, S., MORALES, L., AND MERTES, K. B., (1991) *J. Coord. Chem.* **23,** 155–172.
26. BENCINI, A., BIANCHI, A., GARCÍA-ESPANA, E., GIUSTI, M., MANGANI, S., MICHELONI, M., ORIOLI, P., AND PAOLETTI, P. (1987) *Inorg. Chem.* **26,** 3902–3907.
27. CULLINANE, J., GELB, R. I., MARGULIS, T. N., AND ZOMPA, L. J. (1982) *J. Am. Chem. Soc.* **104,** 3048–3053.
28. MARGULIS, T. N., AND ZOMPA, L. J. (1981) *Acta Crystallogr. Sect. B* **37,** 1426–1428.